

## RESEARCH ARTICLE

# Ultra-Compact Efficient Thermally Actuated Mach-Zehnder Modulator Based on VO<sub>2</sub>

SOHRAB MOHAMMADI-POUYAN<sup>1</sup>, MOEIN AFROUZMEHR<sup>2</sup>,  
AND DEREK ABBOTT<sup>3</sup>, (Fellow, IEEE)

<sup>1</sup>School of Electrical and Computer Engineering, Shiraz University, Shiraz 7134851154, Iran

<sup>2</sup>Klipsch School of Electrical and Computer Engineering, New Mexico State University, Las Cruces, NM 88011, USA

<sup>3</sup>School of Electrical and Electronic Engineering, University of Adelaide, Adelaide, SA 5005, Australia

Corresponding author: Sohrab Mohammadi-Pouyan (s.pouyan@shirazu.ac.ir)

**ABSTRACT** Vanadium dioxide (VO<sub>2</sub>) has emerged as a prominent optical phase change material (O-PCM) for creating high performance devices based on hybrid silicon platforms. However, realizing an efficient and compact optical modulator required for Mach-Zehnder interferometer (MZI) structures, still remains a major challenge in active Si-platforms enabled by VO<sub>2</sub>. This is mainly due to the simultaneous variation of both real and imaginary parts of the refractive index during the phase transition process, which is a significant issue. A modified MZI structure is proposed in this paper while the refractive index variation issue is overcome by operating in the wavelength range between 1.5 to 1.6 μm including the optical C-band. An indium tin oxide (ITO) layer is considered as the microheater for the thermal excitation. An optimized triggering signal with an amplitude of 12.5 V along with an arm length of 2.35 μm of the MZI device ( $V_{\pi}L_{\pi} = 30 \text{ V} \cdot \mu\text{m}$ ) established a  $\pi$ -shift at the output of the device. The proposed device has ER > 35 dB at the entire optical C-band and consumes ~26 pJ for modulating a single bit with a delay of 3.5 ns.

**INDEX TERMS** Mach-Zehnder interferometer, optical modulation, phase change material, thermo-optical modulator, vanadium dioxide.

## I. INTRODUCTION

Photonics has enabled new functionalities in photonic integrated circuits (PICs) in recent years with increasing importance due to the introduction of modern optical applications [1] and compatibility with electronic fabrication technology. Standard active devices based on silicon-on-insulator (SOI) platforms have a large footprint and relatively high power consumption [2]. Hybridization silicon-waveguide structures has emerged as an effective solution for the mentioned issues. Optical phase change materials (O-PCMs) such as vanadium dioxide (VO<sub>2</sub>) [3], [4], Ge-Sb-Te (GST) alloys [5], [6], and Ge<sub>2</sub>Sb<sub>2</sub>Se<sub>4</sub>Te<sub>1</sub> (GSST) [2] have become dominant among other materials considered for hybridization. They have become common due to their superior characteristics including compatibility with complementary metal-oxide-semiconductor (CMOS) technology and the tuneability of

their optical characteristics via external excitation [7]. Optical phase change materials are desirable due to their physical and optical properties at the micro- and nano-scale [8]. Note that O-PCM materials generally benefit from a high finite extinction ratio (ER), while they suffer from relatively high insertion loss (IL) [9] that hindered the introduction of devices with high optical performances. Among the OPCMs, vanadium dioxide (VO<sub>2</sub>) has become dominant due to its optical distinct characteristics such as convenient volatile excitation methods that in comparison with other OPCMs, result in devices with low power consumption. Also, it exhibits a substantial variation of the refractive index during a phase transition phenomenon that drastically changes both the real and imaginary parts of the refractive index of VO<sub>2</sub> [10], [11]. This phase transition can be induced, either thermally [3], [12], [13], electrically [14], [15], or optically [16], [17]. As a result, a range of optical devices based on VO<sub>2</sub> including switches [18], [14], metasurfaces [19], [20], polarizers [21], absorption modulators [22], [23], modulators based on

The associate editor coordinating the review of this manuscript and approving it for publication was M. Saif Islam .

resonating structures including micro ring resonator (MRRs) [24] and Bragg gratings [10], and devices for the realization of advanced modulation schemes such as four-level pulse amplitude modulation (PAM4) [25] have been introduced recently.

The phase transition consists of two states namely the high-loss opaque state known as the metallic phase when an external excitation is applied to VO<sub>2</sub> and it is in the low-loss transparent state identified as the dielectric phase when the excitation is removed. Thermal excitation is typically reported due to its robustness among other triggering methods in which VO<sub>2</sub> is in its metallic phase when its temperature rises above 341 K that is known as the critical temperature ( $T_C$ ). Here, the VO<sub>2</sub> phase is reversed to the dielectric phase again when the temperature declines to less than  $T_C$ . The refractive index of VO<sub>2</sub> at the dielectric phase experiences a considerable change from  $3.243 + j0.353$  to  $1.977 + j2.53$  at the metallic phase at a wavelength of  $1.55 \mu\text{m}$  [26].

One of the very first hybrid VO<sub>2</sub>/Si optical devices was introduced for working in the telecom wavelength range with an active length of  $2 \mu\text{m}$  that showed a moderate extinction ratio of 6.5 dB and insertion loss of around 2 dB [27]. There is always a trade-off between the extinction ratio and the insertion loss in VO<sub>2</sub>-based optical absorption modulators [8], [26]. Extensive efforts have been performed to produce a higher extinction ratio with a lower insertion loss by enhancing the optical properties of the hybrid VO<sub>2</sub>/Si waveguides [8]. Although, resonance-based modulators have been introduced to cope with the mentioned issue, these devices usually are highly sensitive to fabrication process parameters that leads to an extremely difficult realization [10]. Among the introduced structures, a robust device with high optical performance such as a Mach-Zehnder modulator (MZM) is absent as it has not yet been reported yet to the best of our knowledge. Thus, we aim to design a compact VO<sub>2</sub>-based MZM that reveals high performance in terms of footprint, power consumption, and optical characteristics in the C-band wavelength range.

The paper is organized as follows. Section II contains three parts that explains the characteristics of the proposed VO<sub>2</sub>-based MZM structure. The introduced structure comprises of VO<sub>2</sub>-based Mach-Zehnder arms that is explained in part II-A. The geometric parameters of the MZM are determined with an optimization drawn in part II-B. The electro-thermal simulations are devoted in part II-C. where an ITO microheater is simulated and the corresponding specifications including the actuating voltage signal, phase-transition delay, and power consumption are determined.

## II. PROPOSED MODULATOR

VO<sub>2</sub>-based Mach-Zehnder modulator (MZM) is illustrated in Fig. 1. The structure consists of a 3-waveguide coupler at the input as the power splitter within VO<sub>2</sub>-based Mach-Zehnder arms. The structure is followed with a power combiner that collects the light from the arms at the output. The substrate and the passivation layers are considered to

be formed based on SiO<sub>2</sub>. The proposed structure utilizes a silicon-based waveguide that supports only a TE polarized propagating mode at the telecommunication wavelength of  $1.55 \mu\text{m}$ . The arms include of the silicon waveguide, VO<sub>2</sub> thin-layers, and an ITO-based microheater that is exploited to heat up the active layer via the Joule heating mechanism to handle the VO<sub>2</sub> phase-transition process. The height and width of the silicon waveguide are labeled with  $h$  and  $w$ , respectively shown in Fig. 2(b). The thickness of the VO<sub>2</sub> layer is represented as  $t_V$ . Also, the width and thickness of the ITO layer are indicated as  $w_I$  and  $t_I$ , respectively. Herein, the carrier concentration of ITO is considered to be  $10^{19} \text{cm}^{-3}$  resulting in a refractive index of  $1.9615 + j0.0059$  at the wavelength of  $1.55 \mu\text{m}$  that is calculated via the Drude-Lorentz model. Here,  $w$ ,  $h$ ,  $w_I$ , and  $t_I$  are chosen to be 500 nm, 200 nm, 600 nm, and 50 nm, respectively. Considering these dimensions, the effective refractive index of the silicon waveguide is simulated to be 2.284 at a wavelength of  $1.55 \mu\text{m}$ . Two pads are utilized for applying an appropriate voltage (indicated as  $V_S$  in Fig. 1(a)) to trigger the modulator. The fabrication process is briefly explained to address the realization of the proposed device. Starting with the Si-waveguide that is followed with the deposition of the VO<sub>2</sub> layers using a standard patterned-lithography associated with different methods including chemical vapor depositing (CVD), sputtering physical vapor deposition (PVD), and molecular beam epitaxy (MBE) [28], and then a layer of SiO<sub>2</sub> is coated on the pre-fabricated structure using a plasma enhanced chemical vapor deposition (PECVD) process within a patterned area to be excluded for the following deposition of the ITO layer as the micro heater. A very similar approach has been reported for fabricating phase shifters actuating with thermal excitation [29], [30].

The MZM core is consists of active and passive arms. The active arm is actuated when an appropriate voltage is applied to its corresponding ITO-layer that causes a thermal excitation denoted as the ON-state. On the other hand, the OFF-state is introduced when no voltage is applied. This is shown in Fig. 1 that the active arm is attached to the pads and consequently the other arm is considered to be passive. The effective refractive index of the arms at ON- and OFF-states are denoted as  $N_{\text{eff},M}$  and  $N_{\text{eff},D}$ , respectively, where the subscript "M" and "D" indicate the metallic phase and dielectric phase, respectively. It can be addressed that tailoring the real part of the effective refractive index ( $n_{\text{eff}}$ ) of VO<sub>2</sub>-based modulators has been always accompanied with the change of its imaginary part ( $k_{\text{eff}}$ ) [26]. Note that a VO<sub>2</sub>-based MZM hasn't been reported yet due to the above mentioned refractive-index-related issue, although a compact MZM can be expected by exploiting the intense variation of  $n_{\text{eff}}$  during the phase transition. Hence, the structure in Fig. 1 is presented to cope with the mentioned issue, where the input light is injected to unbalance the arms to have the output light combined with an equal amplitude in the ON-state. A 3-waveguide coupler is used to inject the input light unevenly with an appropriate ratio to the arms

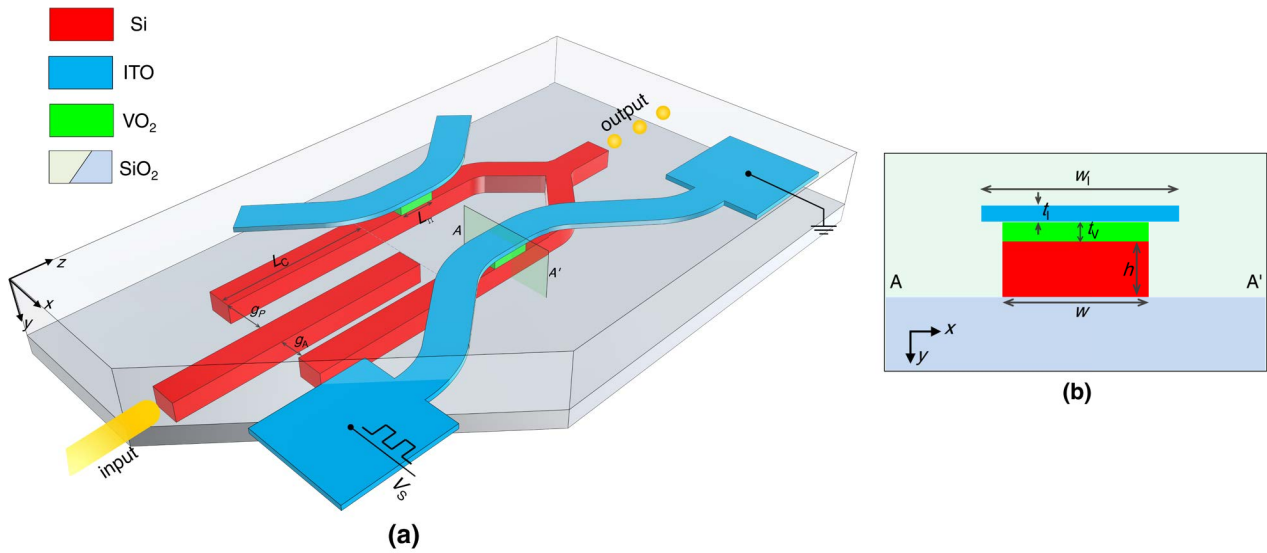


**FIGURE 1.** (a) The perspective three-dimensional schematic view of the proposed device with the geometrical and electrical parameters. (b) The cross-section (AA' plane) of the arms with the geometrical specifications.

to compensate the difference of  $k_{eff}$  between the active and passive arms. This can be achieved by identifying the geometrical properties of the power splitter including distance from the input waveguide to the active arm ( $g_a$ ) and that of the passive arm ( $g_p$ ), and its coupling length ( $L_C$ ). Note that  $L_C$  should be determined properly to maintain a complete light injection into the arms.

**A. MODULATOR ARM DESIGN**

The determination of  $t_v$  must be carried out to accomplish the design of the arm cores. To do so,  $t_v$  is swept from 0 to 200 nm, and at each step of the sweep process, the effective refractive indices have been calculated in both ON- and OFF-states. The result of this simulation is shown in Fig. 2(a, b). To satisfy the single-mode operation, the modulator arm must support only one TE polarized mode as the input silicon waveguide operates. It has been seen in the OFF-state that the modulator always supports both TE and TM polarized modes that has no conflict with the single-mode operation due to the negligible coupling efficiency of the input TE mode to TM mode of the modulator (in order of  $10^{-14}$ ). On the other hand, for  $t_v > 120$  nm, there is a hybrid mode with a notable TE to TM polarization ratio coupled to the input light with a significant efficiency. Thus,  $t_v$  should be chosen less than 120 nm to maintain the single-mode operation criteria. We have introduced a parameter namely  $\Psi$  for the determination of  $t_v$  expressed as  $\Psi = \Delta n_{eff} \times k_{eff,M}/k_{eff,D}$ , where  $\Delta n_{eff} = n_{eff,D} - n_{eff,M}$ . In this equation,  $\Delta n_{eff}$  reflects the length of MZM ( $L_\pi$ ) with a reverse relation. Also,  $k_{eff,M}$  and  $k_{eff,D}$  represent the absorption in the ON-state and the insertion loss in the OFF-state with a direct and reverse relation with the modulator performance, respectively. Fig. 2(c) shows  $\Psi$  as a function of  $t_v$  where the optimum thickness of VO<sub>2</sub> layer is calculated to be nearly

70 nm that satisfies the single-mode operation, as well. By the choice of the optimum value for  $t_v$ ,  $N_{eff,M}$  and  $N_{eff,D}$  are obtained to be  $2.498 + j0.0651$  and  $2.217 + j0.123$ , respectively at the wavelength of  $1.55 \mu\text{m}$ .

**B. OPTIMIZATION OF THE GEOMETRICAL PARAMETERS OF THE MZM**

The injected optical power into the passive arm ( $T_P$ ) and active arm ( $T_A$ ) of MZM by the unbalanced power splitter is determined by considering  $g_A$ ,  $g_P$ , and  $L_C$ . Note that the power splitter causes an unequal phase at the input of the active and passive arms denoted as  $\phi_A$  and  $\phi_P$ , respectively. Therefore, a phase difference is generated at the input of the arms that is represented as  $\Delta\phi = \phi_A - \phi_B$ . This phase difference should be taken into account during the design process of MZM that is governed by the determination of  $L_\pi$ . The MZM characteristics can be modified by varying  $g_A$  and  $g_P$  that explicitly affect  $L_C$  and  $\Delta\phi$ , and consequently, establishes an implicit change in  $L_\pi$ . The power splitter owns three super modes namely even symmetric super-mode (ESM), odd symmetric super-mode (OSM), and anti-symmetric (ASM) that govern  $L_C$  by their effective refractive indices as follows:

$$L_C = \frac{\lambda}{2(n_{ESM} - n_{OSM})} \tag{1}$$

where  $n_{ESM}$ ,  $n_{OSM}$ , and  $\lambda$  are the effective refractive indices of ESM and OSM, and wavelength, respectively. Also, for having a complete input light coupling into the arms,  $n_{ASM} = \frac{1}{2}(n_{ESM} + n_{OSM})$  should be hold where  $n_{ASM}$  is the effective refractive index of ASM.

The design can be started by determining  $g_A$  or  $g_P$ , and here,  $g_A$  is chosen. To do so, we define a parameter  $G = (g_P - g_A)/g_A$ , and then  $L_C$  and insertion loss (IL) of the coupler can be determined as a function of  $G$  for the different values

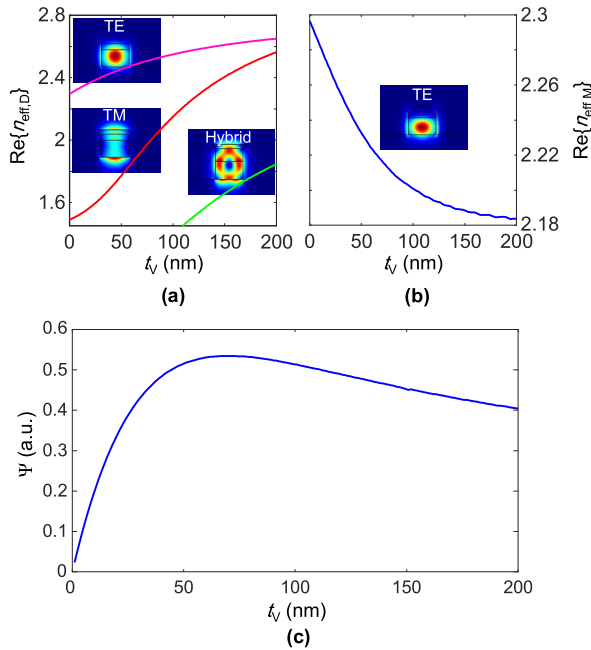


**FIGURE 2.** Refractive index of the modulator as a function of  $t_V$  in (a) ON-state and (b) OFF-state at the wavelength of 1.55  $\mu\text{m}$ . (c)  $\psi$  as a function of  $t_V$ .

of  $g_P$  and  $g_A$ . The result of these calculations are shown in Fig. 3(d, e). Hence, for a compact device with  $\text{IL} < 1$  dB,  $g_A$  is considered to be 50 nm.

Afterward,  $g_P$  is swept from 50 nm ( $G = 0$ ) to 200 nm and  $T_A$ ,  $T_P$ , and  $\Delta\phi$  are calculated at each step, and the results are depicted in Fig. 4(a). As is apparent, there is a non-vanishing  $\Delta\phi$  that must be considered during calculating  $L_\pi$  to obtain a total phase difference of  $180^\circ$  between arms. Note that  $\Delta\phi$  can be either compensated or to be considered as a portion of total required  $180^\circ$  phase difference. The first approach suffers from an additional component for  $\Delta\phi$  compensation, while the second method results in a smaller structure, but comes with a slightly higher insertion loss ( $T_{\text{OFF}}$ ) as it is considered for our design. Based on the transfer matrix method (TMM), The total optical power transmission ( $T$ ) can be determined by multiplying the transfer matrix of each component of the structure namely input power splitter ( $\mathbf{Y}_{\text{in}}$ ), Mach-Zehnder arm core ( $\mathbf{M}_{\text{MZM}}$ ), and output power combiner ( $\mathbf{Y}_{\text{out}}$ ). The power splitter is consisting of a 3-waveguide coupler while the electric field of each output waveguide has a distinct amplitude and phase. Therefore,  $\mathbf{Y}_{\text{in}}$  can be expressed, as follows:

$$\mathbf{Y}_{\text{in}} = \begin{bmatrix} \sqrt{T_A} e^{-j\phi_A} \\ \sqrt{T_P} e^{-j\phi_P} \end{bmatrix} \quad (2)$$

Note that,  $\mathbf{M}_{\text{MZM}}$  and  $\mathbf{Y}_{\text{out}}$  are determined as follows:

$$\mathbf{M}_{\text{MZM}} = \begin{bmatrix} e^{-j\phi_A} e^{-j(\frac{\alpha_A}{2} L_\pi)} & 0 \\ 0 & e^{-j\phi_P} e^{-j(\frac{\alpha_P}{2} L_\pi)} \end{bmatrix}; \quad \mathbf{Y}_{\text{out}} = \begin{bmatrix} \frac{1}{\sqrt{2}} & \frac{1}{\sqrt{2}} \end{bmatrix} \quad (3)$$

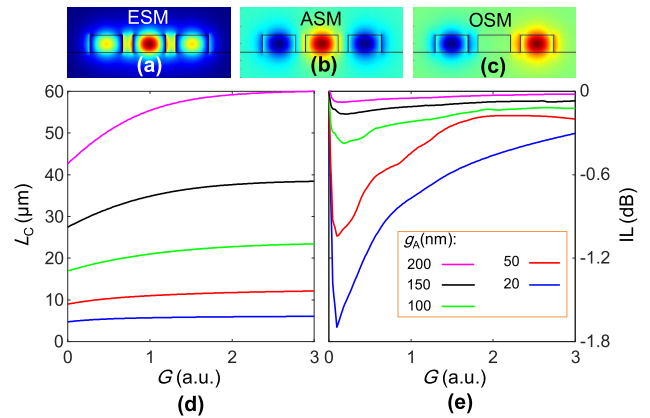


**FIGURE 3.** The electric field profile of the (a) ESM, (b) ASM, (c) OSM, and (d)  $L_C$ . (e) IL as a function of  $G$  for different values of  $g_A$ .

where  $\alpha_A$  and  $\alpha_P$  are the absorption coefficients of the active and passive arms, respectively where the absorption coefficient ( $\alpha$ ) is defined as  $4\pi k_{\text{eff}}/\lambda$ . The following equation describes the relation between the input and output of the electrical field of the device:

$$\mathbf{E}_{\text{out}} = \mathbf{Y}_{\text{out}} \mathbf{M}_{\text{MZM}} \mathbf{Y}_{\text{in}} \mathbf{E}_{\text{in}} \quad (4)$$

where  $\mathbf{E}_{\text{in}}$  and  $\mathbf{E}_{\text{out}}$  denote the electric field of the traveling wave at the device input and output, respectively. Thus, the total optical transmission of the device is calculated as follows:

$$T = \left| \frac{\mathbf{E}_{\text{out}}}{\mathbf{E}_{\text{in}}} \right|^2 \quad (5)$$

Combining (5), (4), (3), and (2) leads to following equation:

$$T = \frac{1}{2} T_A e^{-\alpha_A L_\pi} + \frac{1}{2} T_P e^{-\alpha_P L_\pi} + \sqrt{T_A T_P} e^{-\left(\frac{\alpha_A + \alpha_P}{2}\right) L_\pi} \times \cos\left(\Delta\phi + 2\pi L_\pi \frac{\Delta n_{\text{eff}}}{\lambda}\right) \quad (6)$$

In the ON-state, the following equation should be held to satisfy the destructive interference condition in our designed MZM:

$$\Delta\phi + 2\pi L_\pi \frac{\Delta n_{\text{eff}}}{\lambda} = \pi. \quad (7)$$

We have used Eq. 6 and Eq. 7 to calculate  $L_\pi$  and the total transmission of the device in the ON-state ( $T_{\text{ON}}$ ) as a function of  $g_P$ , and the results are illustrated in Fig. 4(b). It specifies that for  $g_P \approx 98$  nm, the destructive interference condition is fulfilled, and hence, the maximum performance is obtained. Here, we have considered  $g_P$  as its optimum value having corresponding  $L_\pi = 2.35 \mu\text{m}$  and  $L_C = 11 \mu\text{m}$ .

The short distance (650 nm) between arms must be maintained to achieve a compact device. This reduced distance potentially causes a disturbance in the modulation process due to the optical power coupling phenomena between arms. To examine this issue, the coupling efficiency between the arms in both ON- and OFF-states are calculated. To do so,

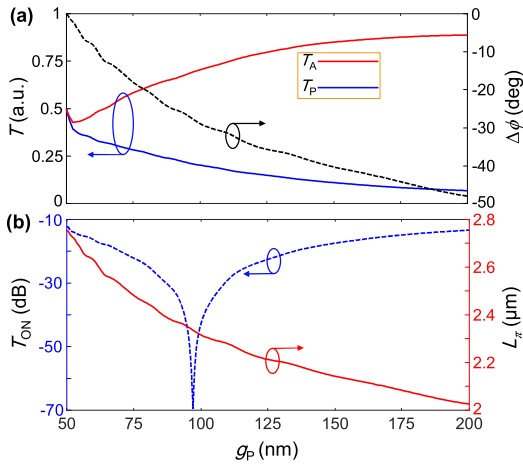


FIGURE 4. (a)  $T_A$ ,  $T_P$ , and  $\Delta\phi$ , (b)  $T_{ON}$  and  $L_\pi$  as a function of  $g_p$ .

the perturbed super-modes established in the vicinity of the arms in the structure must be calculated in both operating states. The percentage of the optical power that couples from one arm to the other can be estimated using  $p(L_\pi) = 100 \sin^2\left(\frac{\pi}{\lambda} L_\pi \Delta n_{\text{eff}}\right)$  where  $\Delta n_{\text{eff}}$  is the difference of the effective refractive indices of the super-modes.

For the OFF-state,  $P(L_\pi)$  is calculated to be  $\sim 2.3 \times 10^{-6}\%$  confirming a very low coupling efficiency between arms that can be neglected. On the other hand, in the ON-state, simulations show that none of the arm's optical modes are perturbed at the distance of 650 nm between arms due to a very high difference in the effective refractive indices in the metallic and dielectric phases. Thus, no super-mode will be established in the structure based on two arms. It can be deduced that there is no optical coupling between arms of the MZM in the ON-state. This argument addressed no disturbance in the modulation performance due to the short distance between arms. The optical properties of the designed MZM within the 3D-FDTD simulations including optical power output spectrum and the electric field distribution of the propagating light are represented in Fig. 5 and Fig. 6, respectively. The insertion loss of the MZM is simulated to be about 7 dB at the wavelength of  $1.55 \mu\text{m}$  and the total transmission in ON- and OFF-states of MZM at the entire simulated wavelength range from  $1.5 \mu\text{m}$  to  $1.6 \mu\text{m}$  (includes the entire optical C-band) remains less than  $-35$  dB and greater than  $-8$  dB, respectively. The thermoelectric characterization and optimizations will be discussed in the next section.

### C. DEVICE THERMAL CHARACTERIZATION

Here, the feasibility of phase transition of the VO<sub>2</sub> layer placed on the top of the active arm of the proposed MZM designed in section II-A is investigated. The thermal excitation for the phase transition is induced by Joule heating mechanism. The multiphysics electro-thermal simulations using the 3D finite element method (3D-FEM) are performed based on the material parameters including material density, thermal conductivity, and heat capacity.

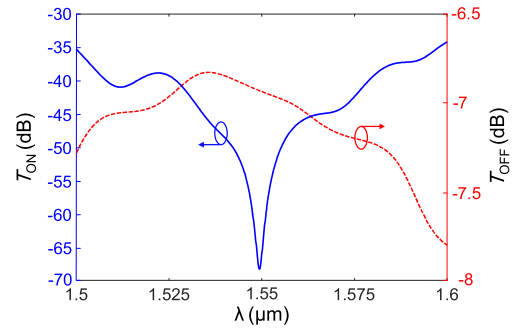


FIGURE 5. The output optical power of MZM in both ON- and OFF-states as a function of wavelength in the range of  $1.5 \mu\text{m} < \lambda < 1.6 \mu\text{m}$ .

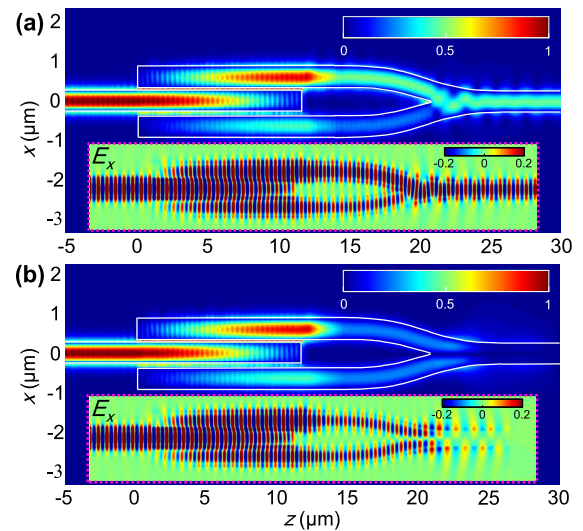
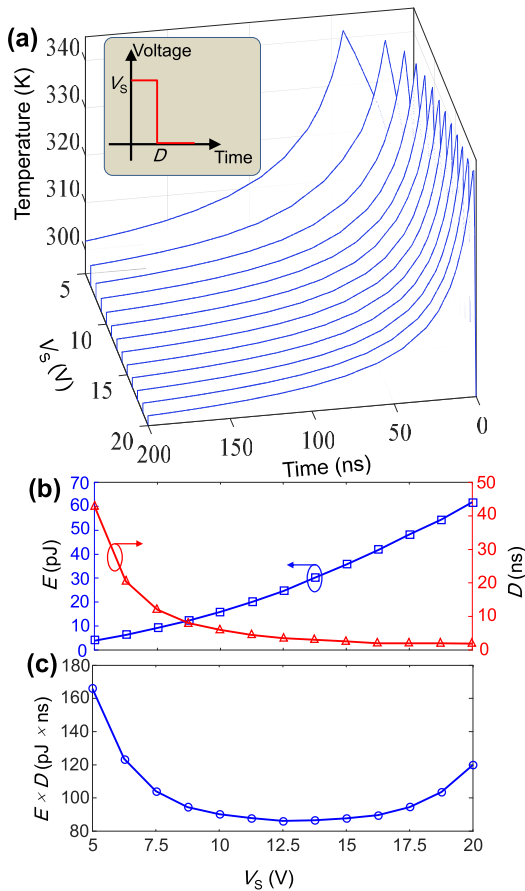


FIGURE 6. The optical electric field distribution at the wavelength of  $1.55 \mu\text{m}$  in the (a) OFF-state and (b) ON-state. The in-set figures are provided to show the dominant electric field ( $E_x$ ) distribution in both corresponding states where the destructive interference in the ON-state ( $180^\circ$  phase difference between arms) at the output of the device is recognizable.

These thermal parameters of ITO, VO<sub>2</sub>, SiO<sub>2</sub> and Si are reported [29], [31], [32]. Note that, ITO is considered as the conductive material of choice for the heater and electrodes. The electrical properties of ITO, specifically the electrical resistivity ( $\rho$ ) required for the calculations are defined by its free carrier concentration. Particularly, for a given carrier concentration of  $10^{19} \text{ cm}^{-3}$ ,  $\rho$  is reported as  $0.0016 \Omega \cdot \text{cm}$  according to experimental measurements [33]. As mentioned earlier, applying an appropriate voltage pulse to the ITO heater makes it warm which establishes the phase transition of VO<sub>2</sub> layer of the active arm when the temperature escalates above the critical temperature ( $T_C = 341 \text{ K}$ ). Various voltages are applied to the ITO heater from 5 to 20 V, and the simulations are kept running until the coolest regions reach 341 K to ensure a complete phase transition and then the applied voltage will be dropped to zero.

The result of the simulations specifies the pulse duration for each applied signal at the mentioned voltage range. The lowest-temperature region of VO<sub>2</sub> as a function of time for



**FIGURE 7.** (a) The lowest-temperature region of VO<sub>2</sub> as a function of time for different applied voltages. The inset figure shows the electrical properties of the trigger signal including amplitude and pulse duration. (b)  $E$  and  $D$ . (c)  $E \times D$  as a function of  $V_s$ .

different applied voltages is plotted in Fig. 7(a) that meets the total phase transition condition. Note that the energy-delay product is an imperative factor for determining the efficiency in digital systems. The necessary energy ( $E$ ), delay time ( $D$ ), and their product ( $E \times D$ ) for reaching the critical temperature at each voltage step are simulated and depicted in Fig. 7(b, c). It can be seen from Fig. 7(c) that the minimum  $E \times D$  product is obtained at  $V_s = 12.5$  V corresponding to  $E \approx 26$  pJ and  $D \approx 3.5$  ns.

Note that  $V_\pi L_\pi$  is considered as a figure of merit to express the electro-optic performance of Mach-Zehnder modulators. Here, the  $V_\pi L_\pi$  measure is calculated to be  $\sim 30$  V  $\cdot$   $\mu\text{m}$  by considering  $V_\pi = V_s = 12.5$  V and  $L_\pi = 2.35$   $\mu\text{m}$ .

Compact-MZM devices have been reported previously including a plasmonic-MZM with a  $V_\pi L_\pi$  of almost 60 V  $\cdot$   $\mu\text{m}$  with experimental results showing almost the same IL, but with an approximate ER of 6 dB [34] in comparison with the proposed MZM in this work. Also, an ITO-MZM has been introduced earlier with  $V_\pi L_\pi$  of 63 V  $\cdot$   $\mu\text{m}$  while it showed a fairly low ER of 2.2 dB [35]. A hybrid platform has been utilized to come up with an experimental design of an MZM based on lithium niobate and silicon nitride thin-film. Their device offered a  $V_\pi L_\pi$  of 2.11 V  $\cdot$  cm with IL

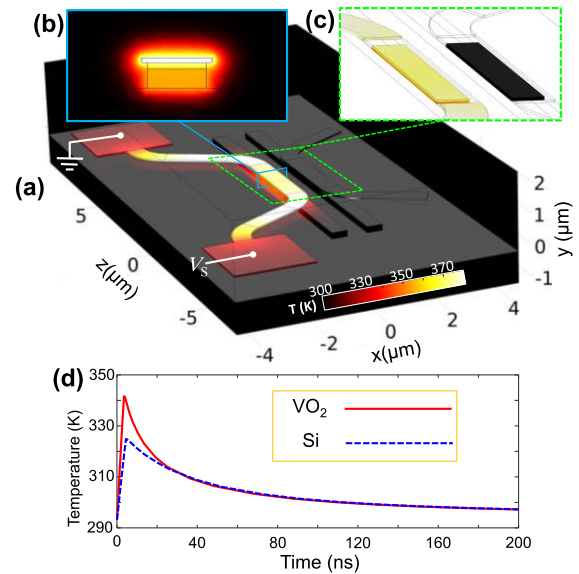


**FIGURE 8.** The thermal distribution profile of (a) the entire device. (b) the active arm (cross-section distinguished by solid-line). (c) both arms (area distinguished by dash-line). (d) The temperature of the coolest region of active VO<sub>2</sub> layer and average temperature of Si-waveguide as a function of time for an appropriate actuation signal.

and ER of 5.4 dB and 30 dB, respectively [36]. Moreover, a graphene-based MZM is notable with an ER of nearly 35 dB that is designed with  $V_\pi L_\pi$  of 44 V  $\cdot$   $\mu\text{m}$  [37]. Finally, a 5  $\mu\text{m}$  integrated MZM with photonic crystal phase shifter in a p-i-n diode structure is represented. This device requires nearly 1 V as the operating voltage with an insertion loss less than 1 dB [38]. The temperature distribution profile of the device after 3.5 ns of applying the trigger signal of 12.5 V is illustrated in Fig. 8. As the simulation result indicates, the stimulation of the active arm does not affect the temperature distribution of the passive arm (Fig. 8(c)). Thus, the phase transition occurred only for the active arm and no phase-change is observed in the passive arm. The average temperature of the Si-waveguide is also depicted in Fig. 8(d) that implies the temperature variation of the Si-waveguide will not exceed 20 K. This low-temperature variation in the Si-waveguide is accompanied by a low thermo-optic coefficient of  $dn/dT = 1.8 \times 10^{-4}$  [39] results in a negligible variation in the refractive index of silicon.

The same argument is applied to the ITO-layer, as well. The thermal considerations do not noticeably impact the optical characterization of Si and ITO. Therefore, the results remain approximately unchanged. Note that ITO-based heaters have been extensively explored [29], [30], [31] where the effect of passivation-coating material, distance of heater from the phase shifter, and the specifications of the heater on the thermal characterization have been studied extensively.

### III. CONCLUSION

We have proposed an MZI structure to realize modulation using VO<sub>2</sub>-based waveguides as the arms. The device is designed using 3D-FDTD consisting of a 3-waveguide

directional coupler power splitter and a phase shifter. The characteristics of the active waveguide enable the design of a compact device based on the proposed MZM due to employing the intense variation of refractive index in VO<sub>2</sub> during its phase transition. The  $V_{\pi}L_{\pi}$  of nearly 30 V · μm and the power consumption of about 26 pJ are calculated for our MZM with the active length of 2.35 μm. The ITO heater provides the thermal requirements and the electro-thermal characterization including the properties of the actuating voltage signal and phase transition delay of the modulator have been performed using 3D-FEM simulations.

## REFERENCES

- [1] H. Zhang, L. Xu, J. Chen, L. Zhou, B. M. A. Rahman, X. Wu, L. Lu, Y. Xu, J. Xu, J. Song, and Z. Hu, "Ultracompact Si-GST hybrid waveguides for nonvolatile light wave manipulation," *IEEE Photon. J.*, vol. 10, no. 1, pp. 1–10, Feb. 2018.
- [2] F. D. Leonardi, R. Soref, V. M. N. Passaro, Y. Zhang, and J. Hu, "Broadband electro-optical crossbar switches using low-loss Ge<sub>2</sub>Sb<sub>2</sub>Se<sub>4</sub>Te<sub>1</sub> phase change material," *J. Lightw. Technol.*, vol. 37, no. 13, pp. 3183–3191, Jul. 1, 2019.
- [3] S. M. Pouyan, M. Miri, and M. H. Sheikhi, "Design of a CMOS compatible dual polarization four-level optical modulator based on thermally-actuated phase transition of vanadium dioxide," *Photon. Nanostruct. Fundam. Appl.*, vol. 35, Jul. 2019, Art. no. 100710.
- [4] M. Sadeghi, B. Janjan, M. Heidari, and D. Abbott, "Mid-infrared hybrid Si/VO<sub>2</sub> modulator electrically driven by graphene electrodes," *Opt. Exp.*, vol. 28, no. 7, pp. 9198–9207, Mar. 2020.
- [5] A. Mahmoodi, M. Miri, M. H. Sheikhi, and S. Mohammadi-Pouyan, "Design of high extinction ratio, low loss, and compact optical modulators and switches based on GST phase change material," *J. Opt. Soc. Amer. B, Opt. Phys.*, vol. 38, no. 11, pp. 3261–3268, Nov. 2021.
- [6] A. Shadmani, M. Miri, and S. M. Pouyan, "Ultra-wideband multi-level optical modulation in a Ge<sub>2</sub>Sb<sub>2</sub>Te<sub>5</sub>-based waveguide with low power consumption and small footprint," *Opt. Commun.*, vol. 439, pp. 53–60, May 2019.
- [7] J. T. Kim, "CMOS-compatible hybrid plasmonic modulator based on vanadium dioxide insulator-metal phase transition," *Opt. Lett.*, vol. 39, no. 13, pp. 3997–4000, Jul. 2014.
- [8] S. Cuffe, J. John, Z. Zhang, J. Parra, J. Sun, R. Orobchouk, S. Ramanathan, and P. Sanchis, "VO<sub>2</sub> nanophotonics," *APL Photon.*, vol. 5, no. 11, Nov. 2020, Art. no. 110901.
- [9] K. J. Miller, R. F. Haglund, and S. M. Weiss, "Optical phase change materials in integrated silicon photonic devices," *Opt. Mater. Exp.*, vol. 8, no. 8, pp. 2415–2429, Aug. 2018.
- [10] S. Mohammadi-Pouyan, M. Miri, and M. H. Sheikhi, "Design and numerical analysis of a high-performance optical modulator based on Si-VO<sub>2</sub> Bragg grating waveguide," *Appl. Opt.*, vol. 60, no. 5, pp. 1083–1091, Feb. 2021.
- [11] H. W. Verleur, A. S. Barker, Jr., and C. N. Berglund, "Optical properties of VO<sub>2</sub> between 0.25 and 5 eV," *Phys. Rev.*, vol. 172, no. 3, p. 788, Aug. 1968.
- [12] I. Olivares, L. Sánchez, J. Parra, R. Larrea, A. Griol, M. Menghini, P. Homm, L. W. Jang, B. van Bilzen, J. W. Seo, and J. P. Locquet, "Optical switching in hybrid VO<sub>2</sub>/Si waveguides thermally triggered by lateral microheaters," *Opt. Exp.*, vol. 26, no. 10, pp. 12387–12395, May 2018.
- [13] V. Jeyaselvan, A. Pal, P. A. Kumar, and S. K. Selvaraja, "Thermally-induced optical modulation in a vanadium dioxide-on-silicon waveguide," *OSA Continuum*, vol. 3, no. 1, pp. 132–142, Jan. 2020.
- [14] B. Janjan, M. Miri, A. Zarifkar, and M. Heidari, "Design and simulation of compact optical modulators and switches based on Si-VO<sub>2</sub>-Si horizontal slot waveguides," *J. Lightw. Technol.*, vol. 35, no. 14, pp. 3020–3028, Jul. 15, 2017.
- [15] P. Markov, R. E. Marvel, H. J. Conley, K. J. Miller, R. F. Haglund, and S. M. Weiss, "Optically monitored electrical switching in VO<sub>2</sub>," *ACS Photon.*, vol. 2, no. 8, pp. 1175–1182, Aug. 2015.
- [16] J. K. Clark, Y.-L. Ho, H. Matsui, and J.-J. Delaunay, "Optically pumped hybrid plasmonic-photonic waveguide modulator using the VO<sub>2</sub> metal-insulator phase transition," *IEEE Photon. J.*, vol. 10, no. 1, pp. 1–9, Feb. 2018.
- [17] J. Parra, T. Ivanova, M. Menghini, P. Homm, J.-P. Locquet, and P. Sanchis, "All-optical hybrid VO<sub>2</sub>/Si waveguide absorption switch at telecommunication wavelengths," *J. Lightw. Technol.*, vol. 39, no. 9, pp. 2888–2894, May 1, 2021.
- [18] L. Sánchez, S. Lechago, A. Gutierrez, and P. Sanchis, "Analysis and design optimization of a hybrid VO<sub>2</sub>/silicon 2×2 microring switch," *IEEE Photon. J.*, vol. 8, no. 2, pp. 1–9, Apr. 2016.
- [19] M. Jiang, F. Hu, L. Zhang, B. Quan, W. Xu, H. Du, D. Xie, and Y. Chen, "Electrically triggered VO<sub>2</sub> reconfigurable metasurface for amplitude and phase modulation of terahertz wave," *J. Lightw. Technol.*, vol. 39, no. 11, pp. 3488–3494, Jun. 2021.
- [20] J.-K. Yang and H.-S. Jeong, "Switchable metasurface with VO<sub>2</sub> thin film at visible light by changing temperature," *Photonics*, vol. 8, no. 2, p. 57, Feb. 2021.
- [21] M. Heidari, V. Faramarzi, Z. Sharifi, M. Hashemi, S. Bahadori-Haghighi, B. Janjan, and D. Abbott, "A high-performance TE modulator/TM-pass polarizer using selective mode shaping in a VO<sub>2</sub>-based side-polished fiber," *Nanophotonics*, vol. 10, no. 13, pp. 3451–3463, Aug. 2021.
- [22] P. Muñoz, G. Micó, L. A. Bru, D. Pastor, D. Pérez, J. D. Doménech, J. Fernández, R. Baños, B. Gargallo, R. Alemany, and A. M. Sánchez, "Silicon nitride photonic integration platforms for visible, near-infrared and mid-infrared applications," *Sensors*, vol. 17, no. 9, p. 2088, Sep. 2017.
- [23] H. M. K. Wong and A. S. Helmy, "Performance enhancement of nanoscale VO<sub>2</sub> modulators using hybrid plasmonics," *J. Lightw. Technol.*, vol. 36, no. 3, pp. 797–808, Feb. 1, 2018.
- [24] J. D. Ryckman, V. Diez-Blanco, J. Nag, R. E. Marvel, B. K. Choi, R. F. Haglund, and S. M. Weiss, "Photothermal optical modulation of ultra-compact hybrid Si-VO<sub>2</sub> ring resonators," *Opt. Exp.*, vol. 20, no. 12, pp. 13215–13225, Jun. 2012.
- [25] S. Mohammadi-Pouyan, M. Miri, and M. H. Sheikhi, "Design of a vanadium dioxide-based dual-polarization optical PAM<sub>4</sub> modulator," *J. Opt. Soc. Amer. B, Opt. Phys.*, vol. 35, no. 12, pp. 3094–3103, Dec. 2018.
- [26] B. Wu, A. Zimmers, H. Aubin, R. Ghosh, Y. Liu, and R. Lopez, "Electric-field-driven phase transition in vanadium dioxide," *Phys. Rev. B, Condens. Matter*, vol. 84, no. 24, Dec. 2011, Art. no. 241410.
- [27] R. M. Briggs, I. M. Pryce, and H. A. Atwater, "Compact silicon photonic waveguide modulator based on the vanadium dioxide metal-insulator phase transition," *Opt. Exp.*, vol. 18, no. 11, pp. 11192–11201, May 2010.
- [28] Y. Ke, S. Wang, G. Liu, M. Li, T. J. White, and Y. Long, "Vanadium dioxide: The multistimuli responsive material and its applications," *Small*, vol. 14, no. 39, Sep. 2018, Art. no. 1802025.
- [29] J. Parra, J. Hurtado, A. Griol, and P. Sanchis, "Ultra-low loss hybrid ITO/Si thermo-optic phase shifter with optimized power consumption," *Opt. Exp.*, vol. 28, no. 7, pp. 9393–9404, Mar. 2020.
- [30] H. Taghinejad, S. Abdollahramezani, A. A. Eftekhari, T. Fan, A. H. Hosseini, O. Hemmatyar, A. E. Dorche, A. Gallmon, and A. Adibi, "ITO-based microheaters for reversible multi-stage switching of phase-change materials: Towards miniaturized beyond-binary reconfigurable integrated photonics," *Opt. Exp.*, vol. 29, no. 13, pp. 20449–20462, Jun. 2021.
- [31] G. V. Chandrashekar, H. L. C. Barros, and J. M. Honig, "Heat capacity of VO<sub>2</sub> single crystals," *Mater. Res. Bull.*, vol. 8, no. 4, pp. 369–374, Apr. 1973.
- [32] B. Janjan, M. Miri, D. Fathi, M. Heidari, and D. Abbott, "Hybrid Si<sub>3</sub>N<sub>4</sub>/VO<sub>2</sub> modulator thermally triggered by a graphene microheater," *IEEE J. Sel. Topics Quantum Electron.*, vol. 26, no. 5, pp. 1–6, Sep. 2020.
- [33] Y. Gui, M. Miscuglio, Z. Ma, M. H. Tahersima, S. Sun, R. Amin, H. Dalir, and V. J. Sorger, "Towards integrated metatronics: A holistic approach on precise optical and electrical properties of indium tin oxide," *Sci. Rep.*, vol. 9, no. 1, Aug. 2019, Art. no. 11279.
- [34] C. Haffner, W. Heni, Y. Fedoryshyn, J. Niegemann, A. Melikyan, D. L. Elder, B. Baeuerle, Y. Salamin, A. Josten, U. Koch, C. Hoessbacher, F. Ducry, L. Juchli, A. Emboras, D. Hillerkuss, M. Kohl, L. R. Dalton, C. Hafner, and J. Leuthold, "All-plasmonic Mach-Zehnder modulator enabling optical high-speed communication at the microscale," *Nature Photon.*, vol. 9, no. 8, pp. 525–528, Aug. 2015.
- [35] R. Amin, R. Maiti, J. K. George, X. Ma, Z. Ma, H. Dalir, M. Miscuglio, and V. J. Sorger, "A lateral MOS-capacitor-enabled ITO Mach-Zehnder modulator for beam steering," *J. Lightw. Technol.*, vol. 38, no. 2, pp. 282–290, Jan. 15, 2020.
- [36] A. N. R. Ahmed, S. Nelan, S. Shi, P. Yao, A. Mercante, and D. W. Prather, "Subvolt electro-optical modulator on thin-film lithium niobate and silicon nitride hybrid platform," *Opt. Lett.*, vol. 45, no. 5, pp. 1112–1115, 2020.

- [37] L. Yang, T. Hu, R. Hao, C. Qiu, C. Xu, H. Yu, Y. Xu, X. Jiang, Y. Li, and J. Yang, "Low-chirp high-extinction-ratio modulator based on graphene-silicon waveguide," *Opt. Lett.*, vol. 38, no. 14, pp. 2512–2515, Jul. 2013.
- [38] A. Govdali, M. C. Sarihan, U. Karaca, and S. Kocaman, "Integrated optical modulator based on transition between photonic bands," *Sci. Rep.*, vol. 8, no. 1, p. 1619, Jan. 2018.
- [39] J. Komma, C. Schwarz, G. Hofmann, D. Heinert, and R. Nawrodt, "Thermo-optic coefficient of silicon at 1550 nm and cryogenic temperatures," *Appl. Phys. Lett.*, vol. 101, no. 4, Jul. 2012, Art. no. 041905.



**MOEIN AFROUZMEHR** received the M.Sc. degree in electrical engineering from Shiraz University, Shiraz, Iran, in 2018. He is currently pursuing the degree with New Mexico State University (NMSU). He was a Research Fellow on the design and fabrication of nano-devices at Shiraz University for three years. His research interests include sensors, optical switches and modulators, and nano-photonics devices. Recently, he became interested in data science. He works on the data side, including numerical modeling and analysis.



**DEREK ABBOTT** (Fellow, IEEE) was born in South Kensington, London, U.K. He received the B.Sc. degree (Hons.) in physics from Loughborough University, U.K., in 1982, and the Ph.D. degree in electrical and electronic engineering from the University of Adelaide, Australia, in 1997, under the supervision of K. Eshraghian and B. R. Davis. His research interests include the areas of multidisciplinary physics and electronic engineering applied to complex systems. His research programs span a number of areas of stochastics, game theory, photonics, energy policy, biomedical engineering, and computational neuroscience. He is a fellow of the Institute of Physics, U.K., and an Honorary Fellow of Engineers Australia. He received a number of awards, including the South Australian Tall Poppy Award for Science, in 2004, the Australian Research Council Future Fellowship, in 2012, the David Dewhurst Medal, in 2015, the Barry Inglis Medal, in 2018, and the M. A. Sargent Medal for eminence in engineering, in 2019. He was the Editor and/or a Guest Editor of a number of journals, including the IEEE JOURNAL OF SOLID-STATE CIRCUITS, *Journal of Optics B*, *Chaos, Fluctuation and Noise Letters*, PROCEEDINGS OF THE IEEE, the IEEE PHOTONICS JOURNAL, and *PNAS Nexus*. He has served on the board for PROCEEDINGS OF THE IEEE, and is currently on the Editorial Boards for *Scientific Reports* (Nature), *Royal Society OS*, *Frontiers in Physics*, *Oxford Open Materials Science* and IEEE ACCESS. He serves on the IEEE Publication Services and Products Board (PSPB) and is the current Editor-in-Chief (EIC) for IEEE ACCESS.

...



**SOHRAB MOHAMMADI-POUYAN** received the M.Sc. degree in electronics from the University of Tehran, Tehran, Iran, in 2015, and the Ph.D. degree in electronics with a minor in nano-devices from Shiraz University, Shiraz, Iran. He is currently a Research Fellow with Shiraz University, working on optical photonic devices. His research interests include the analysis and design of integrated nanophotonic devices and on-chip integration of novel materials.